THE JOURNAL OF PHYSICAL CHEMISTRY B

Article

Cite This: J. Phys. Chem. B 2019, 123, 7676−7686

pubs.acs.org/JPCB

Folding and Dynamics Are Strongly pH-Dependent in a Psychrophile Frataxin

Rodolfo M. González-Lebrero,[*,†,‡] Lucas Defelipe,[§,∥] Carlos Modenutti,[§,∥] Adrian E. Roitberg,[⊥] Nicolas A. Batastini,[†] Martín E. Noguera,[†] Javier Santos,[#] and Ernesto A. Roman[*,‡,∥]

[†]Facultad de Farmacia y Bioquímica, Departamento de Química Biológica, Universidad de Buenos Aires, Buenos Aires C1113AAD, Argentina

[‡]Consejo Nacional de Investigaciones Científicas y Técnicas, Instituto de Química y Fisicoquímica Biológicas, Buenos Aires C1113AAD, Argentina

[§]Facultad de Ciencias Exactas y Naturales, IQUIBICEN, [∥]Facultad de Ciencias Exactas y Naturales, Departamento de Química Biológica, and [#]Departamento de Fisiología y Biología Molecular y Celular, Facultad de Ciencias Exactas y Naturales, Instituto de Biociencias, Biotecnología y Biomedicina (iB3), Universidad de Buenos Aires, Intendente Güiraldes 2160—Ciudad Universitaria, 1428EGA C.A.B.A., Argentina

[⊥]Department of Chemistry, University of Florida, Gainesville, Florida 32611, United States

Supporting Information

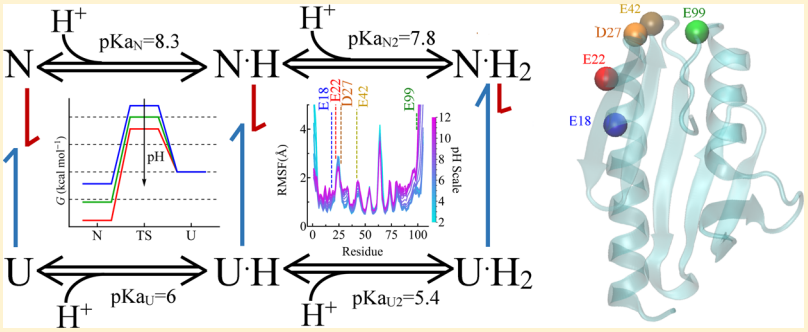

ABSTRACT: Protein dynamics, folding, and thermodynamics represent a central aspect of biophysical chemistry. pH, temperature, and denaturant perturbations inform our understanding of diverse contributors to stability and rates. In this work, we performed a thermodynamic analysis using a combined experimental and computational approach to gain insights into the role of electrostatics in the folding reaction of a psychrophile frataxin variant from *Psychromonas ingrahamii*. This folding reaction is strongly modulated by pH with a single, narrow, and well-defined transition state with ∼80% compactness, ∼70% electrostatic interactions, and ∼60% hydration shell compared to the native state (α_D = 0.82, α_H = 0.67, and $\alpha_{\Delta C_p}$ = 0.59). Our results are best explained by a two-proton/two-state model with very different pK_a values of the native and denatured states (∼5.5 and ∼8.0, respectively). As a consequence, the stability strongly increases from pH 8.0 to 6.0 ($|\Delta\Delta G°| = 5.2$ kcal mol^{-1}), mainly because of a decrease in the $T\Delta S°$. Variation of $\Delta H°$ and $\Delta S°$ at pH below 7.0 is dominated by a change in $\Delta H_f^‡$ and $\Delta S_f^‡$, while at pH above 7.0, it is governed by $\Delta H_u^‡$ and $\Delta S_u^‡$. Molecular dynamics simulations showed that these pH modulations could be explained by the fluctuations of two regions, rich in electrostatic contacts, whose dynamics are pH-dependent and motions are strongly correlated. Results presented herein contribute to the understanding of the stability and dynamics of this frataxin variant, pointing to an intrinsic feature of the family topology to support different folding mechanisms.

INTRODUCTION

The study of protein dynamics, folding, and thermodynamics represents a central aspect of modern biophysical chemistry. In the last 2 decades, polymer theories combined with experimental biochemistry led to plausible explanations on the mechanisms through which the native structure of natural proteins is achieved.[1−3] However, the analysis of folding kinetics and thermodynamics does not always lead to a unique interpretation of the folding mechanism. In this sense, the energy landscape theory and the principle of minimal frustration give a framework for the study of these effects in protein dynamics.[4−8] Although proteins with similar topologies share a similar folding mechanism, they might proceed through different pathways; local energy minima due to transient contacts can form small rugosities in the landscape, giving rise to partially folded conformations, oligomerization, and off-

Received: June 21, 2019
Revised: August 12, 2019
Published: August 13, 2019

DOI: 10.1021/acs.jpcb.9b05960
J. Phys. Chem. B 2019, 123, 7676−7686

pathway conformations, among other phenomena. This suggests that folding funnel topography is tunable by sequence modifications.

Environmental cell conditions, such as internal pH among others, affect protein dynamics and stability. The acidic or basic residues in a protein sequence redound in a net charge that varies with the protonation state related to the residue pK_a and internal pH. Protonation/deprotonation can, at short distances, influence active site catalysis and, at longer distances, take part in oligomerization, conformational changes, and other dynamic events, such as intrinsic protein dynamics and folding reactions. In the latter case, favorable and unfavorable interactions are formed as a consequence of the electrostatic potential at each pH, which has a consequence in the thermodynamic and kinetic stability in that condition.

Frataxin (FXN) is a highly conserved member of the CyaY protein family. Although bacterial variant is not essential, it plays an essential role in eukaryotes.[9] Works from different laboratories argue that FXN can participate in iron homeostasis,[10] acting as a donor to heme synthesis and aconitase repair. However, the central role seems to be its participation in the Fe−S cluster assembly as an activator and stabilization of the functional form of cysteine desulfurase. On the other hand, the bacterial CyaY abolishes Fe−S cluster synthesis upon binding to the IscS/IscU protein complex. This action has been recently demonstrated to be counteracted in the presence of high iron concentrations and other proteins that participate in the formation of these clusters.[11−13] The function of FXN is still under active debate.

Even though the sequence identity within the CyaY family ranges between 25 and 50%, the structure topologies of the FXN-characterized variants are conserved. However, there are differences such as the length of the N-terminal region that confers oligomerization properties[14,15] and the length of the C-terminal region (CTR) that contributes to enhancing the global stability.[16−19]

Although structural topology is conserved in the studied FXN variants, they all fold through different mechanisms. While experiments performed with the segment 90−210 of the human variant, which is the folded core of the mature form, were described by a three-state mechanism with a high energy intermediate state,[16] the bacterial FXN from *Escherichia coli* shows a monomeric two-state folded behavior.[19] Additionally, yeast FXN from *Saccharomyces cerevisiae*, which lacks the C-terminus region and has an extension on the N-terminus region, has shown to form oligomers and folds through a broad and smooth free energy barrier.[16,20,21] As can be seen, the folding dynamics of proteins from the CyaY family is quite complex, suggesting that this family is diverse, with differences between folding mechanisms among orthologues.

Sequences from the CyaY protein family are enriched in their content of aspartic and glutamic residues, with a particular bias toward acidic residues in the last portion of the α1 helix and first portion of the β1 strand[22] (Figure S2). This region is the so-called "acid ridge" and is supposed to be mainly involved in the iron binding[23,24] and the consequent modulation of the FXN oligomeric state.[10] When mutational local frustration is analyzed, the acid ridge is enriched in highly frustrated contacts, suggesting that this region is involved in a function−stability trade-off.[7,18] Altogether, these results point to a charge-mediated mechanism in both iron binding and oligomerization state, with a consequence in protein stability.

Thermodynamic stability of the human and *E. coli* FXN variants shows no pH dependence in the range 6−8,[16,19] whereas this dependence is small but significant for the yeast FXN.[20] However, bacterial FXN from *Psychromonas ingrahamii* showed a significant stabilization when pH decreases from 8 to 6, where melting temperature (T_m) varies from 34 to 56 °C and ΔG from 1.3 to 6 kcal/mol.[25] A deep understanding of stability and dynamics modulation in the FXN fold is still needed. The study of sequences and structures of the CyaY family and how these evolved may aid in the understanding of the stability and dynamics determinants in this family.

To study the stability and dynamics correlations, we focused on the FXN of *P. ingrahamii* (pFXN), an extreme psychrophilic sea-ice bacterium, which grows up to −12 °C (generation time of 240 h, strictly psychrophilic: no growth is observed at 15 °C, with optimal growth temperature at 5 °C). We already characterized the crystal structure and aspects of the thermodynamic stability of this variant, showing that it is significantly reduced and highly modulated by pH, in contrast to other proteins from this family.[25] Moreover, the ionic strength increases pFXN stability; however, it does not seem to alter pH modulation, suggesting that both mechanisms of modulation of stability and dynamics are different, at least in the NaCl and pH intervals studied.[25]

In this work, we studied folding dynamics as a function of pH and temperature to gain insights into thermodynamics and kinetics of the pFXN folding mechanism. Fluorescence and circular dichroism (CD) experiments, both in equilibrium and in time-resolved, point to an entropic stabilization of pFXN as a function of pH with, at least, two protons exchanged between native and unfolded conformational ensembles. Additionally, molecular dynamics simulations using explicit solvent constant pH and structure-based models suggest a correlation between pK_a shifts of specific glutamic and aspartic residues of pFXN and their role in the modulation of the free energy landscape. Finally, this work provides insights into the enthalpic and entropic contributions that originate the folding/unfolding barrier and contributes to the understanding of the role of electrostatics in this behavior.

METHODS

Expression and Purification of pFXN. The FXN gene from *P. ingrahamii* was synthesized and subcloned into a pET9b expression plasmid. Bacteria cultures (*E. coli* BL21 (DE3), 2−3 L 2× YT broth, pH 7.2) were grown at 37 °C. Protein expression was induced at DO_{600nm} = 1.0 by the addition of 2% of lactose for 7 h. The concentration of pFXN was determined with UV absorbance using the molar extinction coefficient ε_{280nm} = 16 960 M^{-1} cm^{-1} (Abs_{280nm} 1 mg/mL = 0.73). The purity and oligomeric state of pFXN were checked by size exclusion chromatography coupled to a static light scattering detection, indicating a >99% purity in a monomeric state (Figure S1). For details, see the Supporting Information.

Folding Dynamics Studied by Rapid Mixing Experiments. The procedure uses a rapid-mixing apparatus (SFM-400 from Bio-Logic) attached to a fluorescence (Bio-logic M200) or CD (spectropolarimeter Jasco 810) detector. Folding and unfolding experiments were performed mixing one volume of a solution containing native or unfolded protein with seven volumes of a solution containing different urea concentrations. In addition, unfolding and folding baselines were obtained by mixing native or unfolded protein solution

DOI: 10.1021/acs.jpcb.9b05960
J. Phys. Chem. B 2019, 123, 7676−7686

with buffer or urea at above-denaturation and below-denaturation urea concentration solutions, respectively. On the basis of the full emission spectrum of FXN (305−430 nm) upon excitation at 295 nm in the absence and presence of a high urea concentration at equilibrium, a 320 cutoff filter was used to measure the change on Trp fluorescence (see the Supporting Information of ref 25). CD signal was measured at 225 nm with a band pass of 4 nm using a 0.2 cm path cell. Between 3 and 6 experimental traces were averaged to evaluate the time course at each urea. It is noteworthy that urea dependence of the observed time constant of the folding/unfolding process and equilibrium signals obtained from both Trp fluorescence emission and far UV CD measurements are not significantly different. Altogether, these observations indicate that both techniques report, on average, the same process (Figure S3).

Model Selection. Regression procedures allowed us to define the goodness of the fit of a given equation to the experimental results and to choose among different models by using the Akaike information criterion (AIC)[26] which is defined as

$$\mathrm{AIC} = N \ln(\mathrm{SS}) + 2P \tag{1}$$

where N is the number of data points, P is the number of parameters plus 1, and SS is the sum of the weighted square residual errors. Statistical weights were 1 in all cases. The equation which gave the lower value of AIC was considered the best.

For instance, the average time courses were fitted by nonlinear regression using (a) one exponential, (b) one exponential plus a straight line, or (c) two exponential functions of time. In our case, we found that the best equation, according to AIC, is a single exponential function of time plus a time-independent term as

$$S = (S_0 - S_\infty)\mathrm{e}^{-k_{\mathrm{obs}}t} + S_\infty \tag{2}$$

$$S = (S_\infty - S_0)(1 - \mathrm{e}^{-k_{\mathrm{obs}}t}) + S_0 \tag{3}$$

where S, S_0, and S_∞ are the signals at different times, at $t = 0$, and when t tends to ∞, respectively, and k_{obs} is the observed time constant of the process.

Two-State Model. The analytic solution of the equation derived from the two-state model is a single exponential function of time (as eqs 2 and 3), whereas the coefficient k_{obs}, the signal at equilibrium (S_∞), and the signal at $t = 0$ (S_0) are defined by eqs 4 and 5, respectively

$$k_{\mathrm{obs}} = k_{\mathrm{f}}\,\mathrm{e}^{-m_{\mathrm{f}}[\mathrm{urea}]} + k_{\mathrm{u}}\,\mathrm{e}^{m_{\mathrm{u}}[\mathrm{urea}]} \tag{4}$$

$$S_{(0/\infty)} = \frac{S_{\mathrm{N}} + sm_{\mathrm{N}}[\mathrm{urea}]_{(0/\infty)} + (S_{\mathrm{U}} + sm_{\mathrm{U}}[\mathrm{urea}]_{(0/\infty)})K_{\mathrm{eq}}\,\mathrm{e}^{m_{\mathrm{eq}}[\mathrm{urea}]_{(0/\infty)}}}{1 + K_{\mathrm{eq}}\,\mathrm{e}^{m_{\mathrm{eq}}[\mathrm{urea}]_{(0/\infty)}}} \tag{5}$$

where k_{f} and k_{u} are the folding and unfolding rate constants, while m_{f} and m_{u} are their urea dependence, respectively; S_{N} and S_{U} are the native or unfolded signal; K_{eq} is the equilibrium constant of the folding/unfolding process (calculated as $k_{\mathrm{u}}/k_{\mathrm{f}}$); and m_{eq} is the dependence of the equilibrium constants on urea concentration (calculated as $m_{\mathrm{f}} + m_{\mathrm{u}}$). Notice that the native or unfolded baseline signal varies linearly with urea concentration according to sm_{N} and sm_{U} values. The $(0/\infty)$ subscript identifies the signal at urea concentration at a time equal to 0 or tending to ∞. The values of $\Delta G°$ were calculated as $-RT\ln(K_{\mathrm{eq}})$.

Multiple Perturbation Equilibrium Experiments. Folding/unfolding equilibrium changes were monitored by the CD signal at 220 nm in a buffered medium containing 7.0 μM protein at several pHs (from 6.0 to 8.0) at different temperatures. Denaturation and stabilization experiments were performed with the addition of urea or sorbitol, respectively. The temperature was varied at a rate of 1 °C min^{-1}, and the melting curves were sampled at 2 °C intervals using a cell with a path length of 1 cm.

Equilibrium experiments were analyzed using the Gibbs−Helmholtz equation

$$\Delta G° = \Delta H° - T\Delta S° + \Delta C_p\left(T - T_{\mathrm{o}} - T\ln\left(\frac{T}{T_{\mathrm{o}}}\right)\right) \tag{6}$$

where $\Delta G°$, $\Delta H°$, and $\Delta S°$ are the folding change in Gibbs free energy, enthalpy, and entropy, respectively; ΔC_p is the change in the heat capacity when the protein is folded; and T_{o} is the reference temperature, which was chosen as 25 °C (298,15 K). Combination of eqs 5 and 6 allows a global fit to the data from temperature and urea equilibrium experiments at each pH.

Molecular Dynamics Simulations. *Explicit Solvent Constant-pH Simulations.* For constant-pH molecular dynamics (CpHMD), AMBER package software was used with AMBER99SB force field.[27,28] In all cases, the initial structures were generated from the coordinates of the crystallographic structure of the *P. ingrahamii* FXN (PDB ID 4HS5) obtained by our group.[25] We performed dehydron and water radial distribution analysis. A detailed description of this analysis and the parameters is presented in the original paper of CpHMD simulations[29] (see the Supporting Information).

Structure-Based Simulations. To investigate pFXN folding, we performed structure-based simulations[30,31] with no electrostatic terms included. We used the simulation package GROMACS 4.5.4; the topology, structure, and contact map inputs were calculated using the SMOG server.[18,30] Several constant-temperature runs were carried out and results were analyzed by the weighted histogram analysis method[32] using Q (fraction of native contacts) as the main reaction coordinate.[33] Folding state per residue is defined as the average number of contacts formed by each residue relative to the total number of contacts formed by that residue in the native state; this local parameter is evaluated at different global fractions of native contacts (see the Supporting Information).

RESULTS

Folding and Unfolding of pFXN. Unfolding and folding processes were followed performing stopped-flow experiments at different urea concentrations (0−8 M) and pHs (5.7−8) at 25 °C. In all cases, best fit to each time course was achieved by a decreasing (folding) or increasing (unfolding) single exponential function of time (t) plus a constant term (eqs 2 and 3 and Figure S4). Figure 1A,B shows the best fitting values of observed time constant (k_{obs}) and the normalized signal as a function of urea concentration at different pHs (the best fitting values of the signal at $t = 0$ and when t tends to ∞—S_0 and S_∞, respectively—are shown in Figure S5). It is noteworthy that the fluorescence monitored comes from W59 and W76. The former has 24% of its surface exposed to the solvent, while the latter has 0%, in comparison to the fully exposed Trp residue in

DOI: 10.1021/acs.jpcb.9b05960
J. Phys. Chem. B 2019, 123, 7676−7686

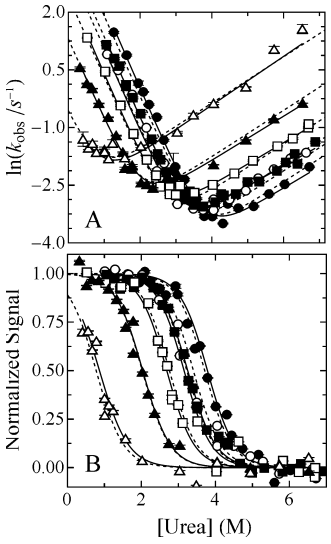

Figure 1. pH dependencies of folding/unfolding denaturation at 298.15 K. Panel A: k_{obs} as a function of urea concentration for different pHs. Panel B: Change of the normalized signal of pFXN at different pHs as a function of urea concentration. Continuous lines are plots of equations derived from the two-state model fit to each pH (5.7 (●); 6.0 (○); 6.15 (◆); 6.5 (□); 7 (▲); and 8 (△)). Dashed lines are plots of equations derived from the two-proton/two-state model fit (Scheme 2) to the whole dataset of both equilibrium and kinetic experiments.

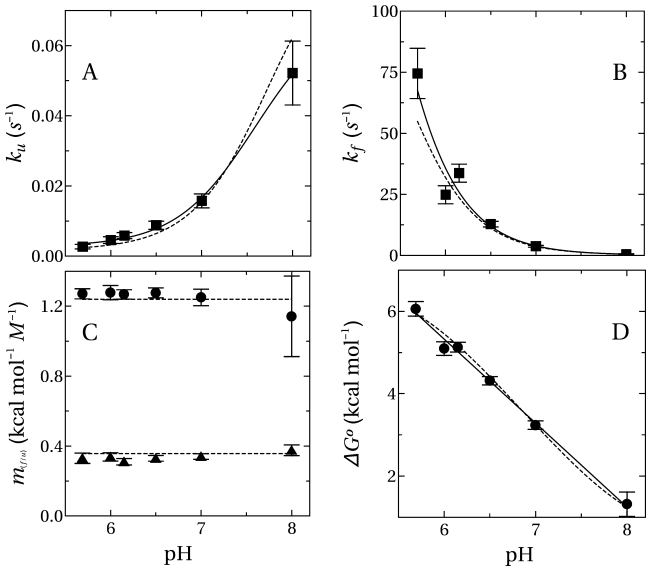

Figure 2. Thermodynamic and kinetic parameters of the pFXN folding reaction. Panels A and B: Best fitting values of folding and unfolding constants from the two-state model (k_f and k_u, respectively) as a function of pH. Continuous lines are plots of a hyperbolic function: $k_f = k_{f,\infty} + (k_{f,0} - k_{f,\infty})K_{f,0.5}/(K_{f,0.5} + [H^+])$ or $k_u = k_{u,0} + (k_{u,\infty} - k_{u,0})[H^+]/(K_{u,0.5} + [H^+])$. Panel C: Best fitting values m_f (●) and m_u (▲) as a function of pH. Panel D: $\Delta G°$ as a function of pH, where the continuous line is the result from eq 7. Dashed lines are the values of k_u, k_f, m-value, and $\Delta G°$ obtained from the equation derived using the two-proton/two-state model (Scheme 2). Error bars are ±standard error of the fitting.

the GWG tripeptide, as calculated with the GETAREA web server. Then, unfolding would originate a significant net change in the solvent accessible area reflected in the shift in the center of mass of Trp emission spectrum and quantum yield of these residues (see also Figure S1 in ref 25).

The best fitting values of the signal at equilibrium (S_∞) display a sigmoidal shape, while k_{obs} dependence on urea shows the typical V-shape without any observable rollover, both compatible with a two-state kinetic mechanism. Both equilibrium and kinetic mid-denaturant concentration ($\Delta G°/m_{eq}$) coincide. It is noteworthy that S_0 values at all urea concentrations coincide with baseline extrapolations of S_∞, indicating that there is no significant change in the signal during the dead time (10 ms) of the reaction, that is, there is no burst phase (Figure S5). As a consequence, the time courses measured and the corresponding k_{obs} reflect the whole process. Thus, equations derived from the two-state model (eqs 4 and 5) were simultaneously fitted to the values of k_{obs}, S_0, and S_∞ at each pH, showing that their dependencies with urea concentration are very well described by the two-state mechanism (continuous line in Figures 1A,B and S2). Best fitting values of rate constant of folding and unfolding (k_f, and k_u) and their urea dependencies (m_f and m_u) obtained at each pH are shown in Figure 2.

The best fitting values of k_f decrease, while k_u increases as pH increases from 5.7 to 8 and can be described by a hyperbolic function of $[H^+]$ (continuous line in Figure 2A,B). Considering that protonation occurs in rapid equilibrium, the $K_{0.5}$ values of the hyperbolic function will be the apparent protonation constant ($-\log K_{0.5} = pK_{aapp}$) for native ($K_{u,0.5}$) and denatured ($K_{f,0.5}$) states being 7.62 ± 0.1 and 4.92 ± 0.2, respectively. This may come from either of the protonable residues participating in the folding and unfolding process, which differ in their identity or their pK_a value.

Figure 2C shows that neither m_f nor m_u significantly changes with a variation of pH. Notice that a small variation of m-values at pH 8 is observed, but this value has lower reliability given the "short" folding limb of the Chevron plot that redounds in a 20% standard error. Given that the m_f- and m_u-values are associated with the change of exposed area in the reaction, the lack of significant variation suggests that neither the transition nor the ground states differ in the exposed surface area between pHs. In this regard, the ratio between m_u and m_{eq} is ~0.2, indicating that there is a slight change of ~20% of the exposed surface between the native and transition states.[34,35]

Gibbs free energy ($\Delta G°$) increases as a function of pH (Figure 2D) and, as described by Tanford et al.,[36,37] when there is a change of the protonation state in a folding transition, equilibrium can be described as a relation between the protonated species in both folded and unfolded states. The slope of the relation between $\Delta G°$ and pH ($\delta\Delta G°/\delta$pH) is directly proportional to the fraction of exchanged protons between folded and unfolded conformations ($\Delta\bar{\nu}_H$).

$$\frac{\partial \Delta G_u^\circ}{\partial \Delta \mathrm{pH}} = -2.303RT\Delta\bar{\nu}_H \qquad (7)$$

Then, the value of the slope in the linear region of the curve is an average $\Delta\nu_H$ in the pH interval analyzed. In our case, $\Delta\bar{\nu}_H$ was 1.49 ± 0.05, indicating that at least two protons are exchanged between folded and unfolded states.

On the basis of our findings, we formulated a minimal kinetic model to explain the results of the folding/unfolding experiments and its pH dependence (Scheme 2).

Considering that protonation is in rapid equilibrium and independent of urea concentration, the model-derived

DOI: 10.1021/acs.jpcb.9b05960
J. Phys. Chem. B 2019, 123, 7676−7686

Scheme 1

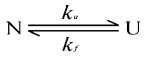

Scheme 2. Two-Proton/Two-State Model[a]

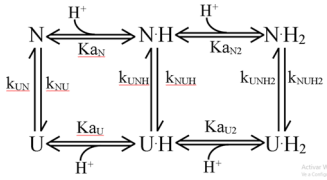

[a] K_{aN} and K_{aN2} are the proton affinities in the native state and K_{aU} and K_{aU2} in the denatured state. The folding/unfolding transition between protonated and deprotonated states of the protein occurs with rate constants named k_{UN}, k_{UNH}, k_{UNH2}, k_{NU}, k_{NUH}, and k_{NUH2}, where subscript NUs or UNs refer to the unfolding or folding process, respectively, and H refers to the protonated state.

equations that account for the changes in S_0 and S_∞ and k_{obs} with urea concentration are equal to eqs 4 and 5 but replace k_f and k_u with $k_{f,app}$ and $k_{u,app}$ given in eqs 8 and 9.

$$k_{u,app} = \frac{K_{aN}K_{aN2}k_{NU} + [H^+]K_{aN2}k_{NUH} + [H^+]^2k_{NUH2}}{[H^+]^2 + [H^+]K_{aN2} + K_{aN}K_{aN2}} \quad (8)$$

$$k_{f,app} = \frac{K_{aU}K_{aU2}k_{UN} + [H^+]K_{aU2}k_{UNH} + [H^+]^2k_{UNH2}}{[H^+]^2 + [H^+]K_{aU2} + K_{aU}K_{aU2}} \quad (9)$$

In order to fit the model-derived equations to k_{obs}, S_0, and S_∞ values, some constraints were taken into account:

(a) The equivalence between the different pathways connecting the same initial and final states places the following additional restrictions on the values of the rate constants: $k_{UN} = \frac{K_{aN}k_{UNH}k_{NU}}{K_{aU}k_{NUH}}$ and $k_{NUH2} = \frac{K_{aN2}k_{UNH2}k_{NUH}}{K_{aU2}k_{UNH}}$

(b) Figure 2C shows that m_{NU} and m_{UN} did not vary significantly as a function of pH; thus, they were considered constant (i.e., $m_{NU} = m_{NUH} = m_{NUH2}$ and $m_{UN} = m_{UNH} = m_{UNH2}$). According to the AIC, this restriction did not diminish the goodness of the fit.

(c) Given that pH dependencies of k_u and k_f are well described by a hyperbola and that there is a linear relation between $\Delta G°$ and pH, identical and independent proton sites were accounted (i.e., $K_{aN2} = 4K_{aN}$ and $K_{aU2} = 4K_{aU}$).

Table 1 shows the best fitting values for each of the constants of Scheme 2. The simulated k_{obs}, S_0, and S_∞ versus urea concentration pH well describe, all at once, the experimental dataset (dashed curves in Figure 1). The following comments seem to be pertinent:

(i) Unfolding rate constants (k_{NU}'s) decrease with the degree of protein protonation (i.e., $k_{NU} \cong k_{NUH} > k_{NUH2}$).

(ii) Conversely, folding rate constants (k_{UN}'s) strongly increase (i.e., $k_{UN} < k_{UNH} < k_{UNH2}$).

(iii) There is a marked change between the native and unfolded pK_{as} (in Table 1, pK_{aN} and pK_{aN2}, pK_{aU} and pK_{aU2}).

(iv) According to the equilibrium constants, the amounts of bi-, mono-, and nonprotonated native state proteins are 61.3, 99.8, and 99.99%, with respect to their unfolded counterpart.

Table 1. Best Fitting Values of Proton Binding and Folding Rate Constants of the Model in Scheme 2

parameter	values ± 1SD	parameter	values ± 1SD
k_{NU} (s^{-1})	0.081 ± 0.011	m_{NU} (kcal mol^{-1} M^{-1})	0.357 ± 0.008
k_{NUH} (s^{-1})	0.085 ± 0.013	m_{UN} (kcal mol^{-1} M^{-1})	1.24 ± 0.016
k_{NUH2} (s^{-1})[a]	(16 ± 2) × 10^{-4}	pK_{aN}	8.32 ± 0.07
k_{UN} (s^{-1})[a]	0.160 ± 0.054	pK_{aN2}[a]	7.78 ± 0.07
k_{UNH} (s^{-1})	35.7 ± 3.8	pK_{aU}	5.99 ± 0.05
k_{UNH2} (s^{-1})	117 ± 23	pK_{aU2}[a]	5.36 ± 0.05

[a] Calculated as was indicated in constraints (a) and (c) of this section.

Multiple Perturbation Analysis. We studied the pH effect on the equilibrium and activation thermodynamics, performing both equilibrium and kinetic experiments, using temperature, urea, and pH perturbations. We evaluated the changes in the folding entropy, enthalpy, and heat capacity using Gibbs−Helmholtz and Kramers-type model equations.

Equilibrium experiments were performed measuring ellipticity at 222 nm (θ_{222}) as a function of temperature (from 3 to 58 °C), urea concentrations (0−7 M), and pH (6.0−8.0) (Figures 3A and S7). Data analyzed independently at each temperature analysis revealed that m_{eq} does not significantly change with temperature. At each pH, fitting combined eqs 5

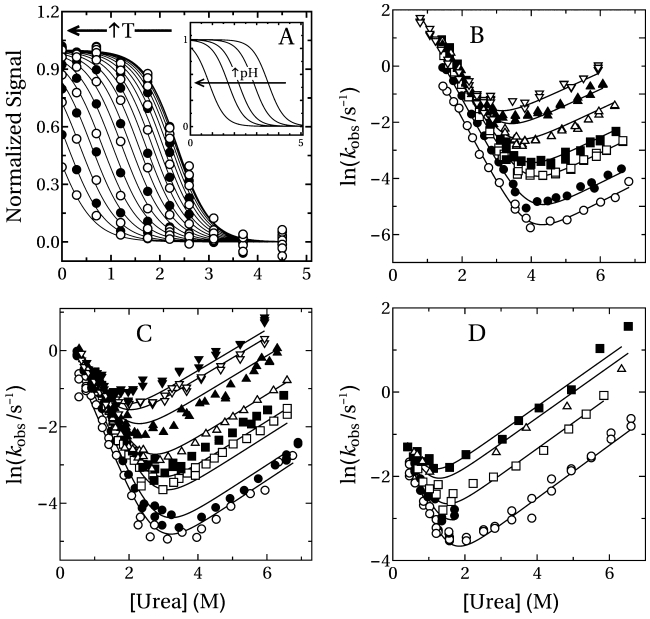

Figure 3. Multiple perturbation experiments. Panel A: Effect of temperature in the urea-induced unfolding at equilibrium for pH 7.38. Continuous lines are the results of the global fit of eqs 5 and 6 to experimental data. The inset shows the result of the global fit to the results at 25 °C for pH 7.99, 7.38, 7.12, 6.66, and 6.04 (complete results are shown in Figure S7). Panels B−D: Experimental values of k_{obs} at different temperatures and urea concentrations (pHs B: 5.86, C: 7.06, and D: 7.90) with the plot of eq 4 using the best fitting values (continuous line). Temperatures in panel B are 7.7 (○), 13.5 (●), 21.2 (□), 24.8 (■), 30.9 (△), 34.8 (▲), and 38.0 (▽), in panel C 5.6 (○), 9.7 (●), 16.3 (□), 19.2 (■), 24.1 (△), 30.4 (▲), 33.2 (▽), and 34.3 (▼), and in panel D are 15.6 (○), 19.3 (●), 21.5 (□), 25.0 (△), and 26.3 (■).

DOI: 10.1021/acs.jpcb.9b05960
J. Phys. Chem. B 2019, 123, 7676−7686

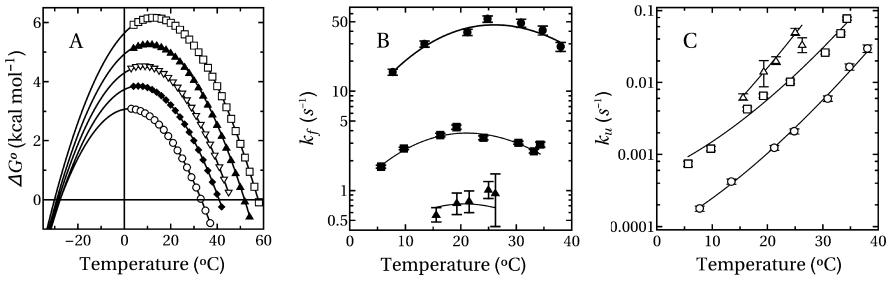

Figure 4. Multiple perturbation: kinetic experiments. Panel A: Unfolding Gibbs free energy as a function of temperature at pH 7.99 (○), 7.38 (■), 7.12 (▽), 6.66 (▲), and 6.04 (□). Lines and points correspond to the value of ΔG calculated from eq 10 at each experimental temperature assessed. Panels B and C: Folding (k_{UN}, closed symbols) and unfolding (k_{NU}, open symbols) rate constants from the two-state model equation at different temperatures for pH 5.86 (circles), 7.06 (squares), and 7.9 (triangles), respectively. Solid lines in panels B and C represent the folding or unfolding term of eq 4 fitted to k_{obs} values at all temperatures at each pH.

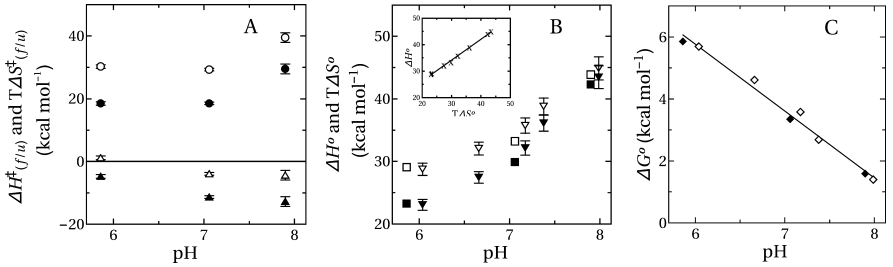

Figure 5. Thermodynamic parameters from equilibrium and kinetic experiments. Panel A: Best fitting values of $\Delta H^{\ddagger}$ (open symbols) and $T\Delta S^{\ddagger}$ (closed symbols) at T_o = 25 °C where circles and triangles are unfolding and folding activation parameters, respectively. Panel B: Equilibrium $\Delta H°$ (open symbols) and $T\Delta S°$ (closed symbols) calculated from equilibrium (squares) and kinetic (inverted triangles) experiments at 25 °C. The inset shows the linear relation between $\Delta H°$ and $T\Delta S°$. Panel C: Gibbs free energy from equilibrium (◇) and kinetic (◆) experiments.

and 6 to experimental data showed no significant change for m_{eq} and ΔC_p (Figure S8). Thus, we considered that both of them were unique for all temperatures and pHs (ΔC_p and m_{eq} equal to 1.83 ± 0.07 kcal mol^{-1} K^{-1} and 1.63 ± 0.04 kcal mol^{-1} M^{-1}, respectively).

At all temperatures, protein stability decreases from pH 6.0 to 8.0. In addition, there is a decrease in the temperature of maximum stability ($\Delta S° = 0$, giving $\Delta G° = \Delta H°$) from 12.7 to 2.2 °C when going from pH 6.0 to 8.0. It is noteworthy that melting temperature (Tm) strongly increases from 33 to 58 °C with a change of pH from 8.0 to 6.0, and conversely, the temperature of cold denaturation remains practically invariant (−28 to −30 °C). When analyzing the enthalpic and entropic contributions to the stability at 25°C, we can observe that both increase with pH (Figure 5B). However, given that the change of $T\Delta S°$ is more pronounced the balance between entropy and enthalpy originates an increase in the stability of pFXN.

By kinetic experiments, k_{obs} of unfolding and refolding reactions were obtained from time courses measured at different urea concentrations (0−7 M) and temperatures (7−38 °C) for pH 5.86, 7.06, and 7.9 (Figure 3B−D), and all of them were described by a single exponential function of time plus a constant term (eqs 2 and 3). In all the conditions tested, Chevron plots are compatible with a two-state folding process (Scheme 1). Notice that at pH 8, as a consequence of the very low C_m at 26 °C, refolding "arms" are extremely short, diminishing the reliability of the quantitative analysis.

Examination of k_f reveals a bell-shaped curve with temperature, while k_u only increases in the assessed range. According to transition state theory, each of the rate constants (k_x) varies with the absolute temperature (T). Combining Kramers-type model for changes of a reaction rate in a viscous solvent[38−42] with the Gibbs−Helmholtz equation (eq 6) results in the following

$$k_{obs} = \frac{\nu\eta_0}{n} e^{-(\Delta H_f^{\ddagger} - \Delta S_f^{\ddagger} T + \Delta C_{pf}^{\ddagger}(T - To - T\ln(\frac{T}{To}))/RT} e^{-m_f[urea]} + \frac{\nu\eta_0}{\eta} e^{-(\Delta H_u^{\ddagger} - \Delta S_u^{\ddagger} T + \Delta C_{pu}^{\ddagger}(T - To - T\ln(\frac{T}{To}))/RT} e^{m_u[urea]} \quad (10)$$

where ν is the k value for a barrierless process and η_0 is the medium viscosity, both at the reference temperature, η is the viscosity at the experimental temperature and urea concentration[43] activation enthalpy ($\Delta H^{\ddagger}$), entropy ($\Delta S^{\ddagger}$), and heat capacity ($\Delta C_p^{\ddagger}$).

Thus, from the variation of k_{obs} with urea concentration and temperature, the values of $\Delta H^{\ddagger}$, $\Delta S^{\ddagger}$ (Figure 5A) and $\Delta C_p^{\ddagger}$ can be obtained. The best fitting values of folding and unfolding m show no significant variation with temperature, indicating that there is neither Hammond nor ground-state effect (see Figure S10). It is often, but not always, observed that the m and the $\Delta C_p^{\ddagger}$ values are in quantitative agreement and reflect solvent exposure of the transition state to either ground states.[35] However, according to the m values, the transition state is 80% native-like, but from the $\Delta C_p^{\ddagger}$ values ($\Delta C_{pf}^{\ddagger}$ and $\Delta C_{pu}^{\ddagger}$ are 1.01 ± 0.06 and 0.70 ± 0.08 kcal mol^{-1} K^{-1}, respectively), it is 59%. These parameters report different phenomena: the former reports on the surface of interaction of the protein with denaturant molecules, whereas the latter reports on changes in the hydration of hydrophobic and polar groups.[44] Activation parameters at each pH are shown in Figure 5.

Unfolding $\Delta H_u^{\ddagger}$ and $T\Delta S_u^{\ddagger}$ contributes more than the folding counterparts to the whole enthalpy and entropy change (Figure 5A). $\Delta S_f^{\ddagger}$ is negative, indicating that the entropy of the

DOI: 10.1021/acs.jpcb.9b05960
J. Phys. Chem. B 2019, 123, 7676−7686

denatured state is higher than the transition state, denoted as $\Delta H_f^{\ddagger}$. $\Delta S_u^{\ddagger}$ and $\Delta H_u^{\ddagger}$ are positive, indicating the opposite when comparing native and transition states. However, $\Delta H_f^{\ddagger}$ at pH 6.0 becomes positive, indicating that transition-state enthalpy is higher compared to the denatured state, reflecting the entropic nature of the transition barrier at that condition.

Water Exchange in the Folding Process. Taking into account the widely recognized role of water in protein folding, we used sorbitol as an osmolyte, which is known to be preferentially excluded from the protein surface (i.e., in the presence of this cosolvent, the protein is preferentially hydrated), to study the role of water in the denaturation process. To this end, we carried out thermal denaturation experiments in the presence of different concentrations of sorbitol (0−0.9 m) at five pH values (6.1−8.0) (Figures 6A and S11). The addition of sorbitol has a stabilizing effect in the studied pH interval, as evidenced by the increase of folding temperatures. The sorbitol-induced increase in stability is less pronounced at pH 6.1 than at the rest of the pH assessed, which is the condition where stability is maximal among assayed conditions.

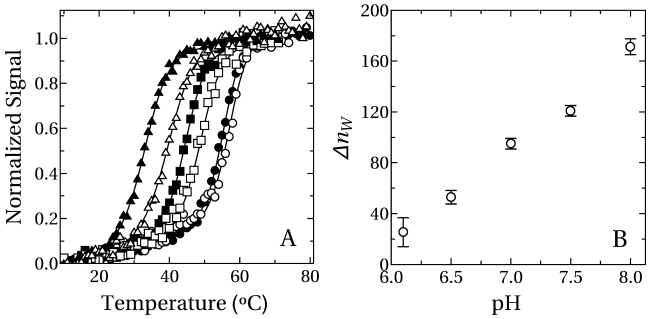

Figure 6. Cosolvent effects and protein hydration changes during folding. Panel A: Normalized signal as a function of temperature for pH 6.1 (○ and ●), 7.0 (□ and ■), and 8.0 (△ and ▲) for thermal melts carried out with (0.904 m, (○, □ and △) or without (●, ■ and ▲) sorbitol. Continuous lines are global fittings of eq 5 to the whole dataset of pH and sorbitol concentrations. Plots for the remaining sorbitol conditions are given in the Supporting Information. Panel B: The number of water molecules exchanged (Δn_W) between folded and unfolded states as a function of pH (obtained as described in the Supporting Information).

Folding transitions were analyzed using the Gibbs−Helmholtz equation (eq 6), and the stability changes at a fixed temperature with sorbitol concentration (preferential interaction parameters) were used to estimate the change in the number of water molecules associated with denaturation of pFXN at the different pH values (see the Supporting Information).[45−47] The number of water molecules exchanged upon pFXN denaturation increases from pH 6.0 to 8.0. This number is around 20−30 at pH 6.1 up to 160−170 at pH 8.0. This may be explained by an effect of electrostatics in the number of water or sorbitol molecules bound to the native and unfolded states. As stated previously, the increase in stability when lowering pH comes from an entropic contribution; this behavior goes in the same direction as the change in the number of bound water molecules in the folding process. Moreover, the slopes of native baselines from equilibrium unfolding curves show a dependence with urea that increases as pH increases from 6.0 to 8.0 (Figure S9). Experiments from de Oliveira and Silva demonstrate that at subdenaturing concentrations, urea binds and dehydrates the protein surface.[48] The more hydrated native state at pH 8.0 suggests that this change in the fluorescence with urea in the native state could be a consequence of protein dehydration. As pFXN ellipticity also varies with urea concentration, this behavior suggests subtle structural and dynamics shift in the native state with urea binding. To discern whether the exchange of water is coupled to entropy or enthalpy contribution has not been possible with our analysis and results.

Fluctuations and Motion Correlations of pFXN. To explore the effect of pH in the dynamics of pFXN, we performed CpHMD from pH 2 to 12. Fluctuations of the main chain, evaluated by root-mean-square fluctuations (RMSFs), showed a significant pH dependency, mainly in loop 1 (stretch from residue 23 to 27) and the CTR (stretch from residue 85 to 105) (Figure S13A). Remarkably, the terminal portion of the C-terminal has shown to be involved in the stability modulation of proteins from the FXN family.[16,19] This suggests that there is a link between the pH-dependent dynamics of this region and pFXN stability. The calculated average RMSF value at each pH reveals that there is a transition in the fluctuations between 6.0 and 9.0 (Figure 7A). This is in accordance with the effect of pH in the k_f (Figure 2A), reflected in the observed native pK_a values (pK_{a1} = 8.32 and pK_{a2} = 7.78, see Table 1).

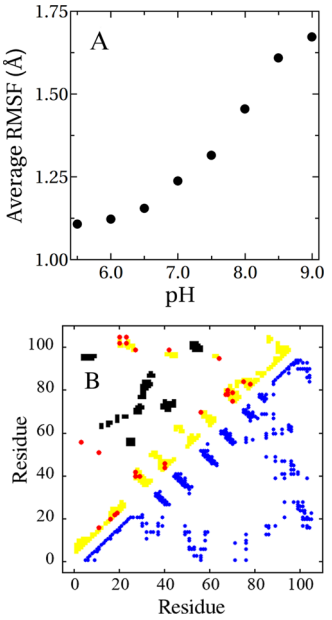

Figure 7. Constant pH and structure-based model simulations. Panel A: Average RMSF as a function of pH. Panel B. Contact map of pFXN (blue circles, lower-right diagonal). Correlated motions are colored in yellow (coefficients above 0.6) and anticorrelated motions are colored in black (coefficients below −0.6). Red circles are the contacts between protonable residues of the protein.

Structure-based model simulations were used to calculate folding free energy profiles of pFXN using umbrella sampling with native contacts as the reaction coordinate. Our results show that there are mainly two energy minima: native (high Q values) and denatured (low Q values) populations (see Figure S13B). In addition, simulations predict an extra very low energetic barrier within the unfolded basin. At all conditions, simulations predict this energetic barrier to be very low, which

DOI: 10.1021/acs.jpcb.9b05960
J. Phys. Chem. B 2019, 123, 7676−7686

is in agreement with a single and conserved limiting step for the folding reaction, as is observed in the experiments.

On the basis of the Q value for the native energy minimum, we clustered structures with $Q \approx 0.7$ to study native state spatial correlations as in elsewhere.[49,50] Cross-correlation coefficients range from a −1 (completely anticorrelated motions) to +1 (completely correlated motions). Unlike covariance matrix elements, they do not bear any information about the magnitude of the motions, which can be small local oscillations as well as large-scale collective motions.[52] We took into account only correlations above 0.6 and anticorrelations below −0.6 (Figure 7B). Interactions of the C-terminus with loop 1 and beta turns 1 and 2 are the most correlated regions of the protein. Interestingly, contacts formed by protonable residues (red spots in Figure 7B) and regions with the highest global RMSF (Figure S13A) are superposed with the region whose motions are correlated (yellow spots in Figure 7B). This indicates that in this case, electrostatics is prone to affect conformational dynamics.

DISCUSSION

Using a combination of thermodynamic and kinetic approaches, we found that pH effects in the folding process are explained through a two-proton/two-state model. It is important to point out that the model was restricted to identical and noninteracting binding sites because of the lack of plateau in the folding and unfolding rate constant isotherms as a function of pH (Figure 2A,B). However, this restriction did not diminish the goodness of the fit. We observed that the decrease in the folding rate with pH is well described with pK_a values for the unfolded state of 5.36 and 5.99, whereas the increase in the unfolding rate is with pK_a values for the native state of 7.78 and 8.32. This difference may come from the following: (a) residues titrated during the folding reaction differ from the ones involved in the unfolding reaction or (b) residues involved in folding and unfolding reactions are the same, but their pK_a is different. As Tanford demonstrated,[38,39] when binding sites are identical and noninteracting, the absolute value of the slope of $\Delta G°$ dependence with pH is equal to the change in the fraction of bound protons between native and unfolded ($\Delta\bar{\nu}_H$). In our case, $\Delta\bar{\nu}_H$ was 1.49 ± 0.05, suggesting that, at least, two protons are exchanged in the folding process. However, this may come, also, from more than two binding sites with a partial occupation. Thus, each of the native and unfolded determined pK_a is unequivocally "apparent" because they may come from many partially occupied sites. If two protons were exchanged, the effect in the unfolding $\Delta G°$ would come from localized titrations; however, if it comes from multiple sites, changes in unfolding $\Delta G°$ would come from a more delocalized surface protonation.

As inferred from a rate-equilibrium free energy relationship (REFER) analysis, α_D (Figure S10) is constant at all conditions $\left(\alpha_D = \frac{\delta\Delta G^{\ddagger} / \delta[\text{denaturant}]}{\delta\Delta G^{0}_{eq} / \delta[\text{denaturant}]}\right)$.[51,52] Thus, all evidence points to a single-narrow and defined transition-state barrier for the reaction. Previous analysis of the FXN orthologue from *S. cerevisiae* has been described as a two-state folding model with a broad transition-state barrier;[20] pFXN is an evidence of the malleability of the CyaY scaffold to support heterogeneous folding mechanisms. Interestingly, the effect of pH on $\Delta G°$ varies with temperature. Then, either temperature induces very subtle alterations in the transition state or REFERs do not fully capture the surface electrostatic effects. Although subtle, these effects influence the thermodynamics of the folding reaction. On the contrary, in pFXN we see no movements in the transition state neither with temperature nor with pH, evidencing that there is no Hammond or ground-state effects (Figure S6). The fact that a single ΔC_p is sufficient to describe the temperature, denaturant, and pH effects reinforces the idea that neither transition nor ground states are changing its energetically/structural state in any condition. The effect of H^+ on the rate and equilibrium constants is related to the respective H^+ binding isotherms.[53] REFER analysis for H^+ binding $\left(\alpha_H = \frac{\delta\Delta G^{\ddagger} / \delta[H^+]}{\delta\Delta G^{0}_{eq} / \delta[H^+]}\right)$ shows that α_H (0.67) and α_D (0.82) are not coincident. Given that k_f and k_u both vary with pH, there is no other possibility that the transition state pK_a differs in both ground states. Thus, at a fixed pH, the position in the binding isotherms is different, yielding a different bound H^+ for transition and ground states.

When analyzing thermodynamic contributions to protein stability, we observe that both $\Delta H°$ and $\Delta S°$ increase when pH increases from 6 to 8. Interestingly, the slope of the linear correlation between them is higher than 1 (inset in Figure 5B, slope = 1.26), indicating that there is not a perfect compensation of $\Delta S°$ and $\Delta H°$ because $T\Delta S°$ varies more pronouncedly than $\Delta H°$. In this vein, at 298.15 K, $T\Delta S°$ varies ∼15 kcal mol^{-1}, while $\Delta H°$ varies only ∼10 kcal/mol, indicating that pFXN is stabilized, mainly from the entropic contribution. Sorbitol stabilization experiments indicated that the number of water molecules exchanged in the folding reaction increases with pH (Figure 6B) probably as a consequence of a change in the electrostatic surface potential related to the pK_a shift of titratable residues. In the same sense, slopes of native baseline dependence with pH suggest a differential hydration of the native state (Figure S9). Given that the solvent is the most populated species in the solution, the main source of entropy change is thought to come from water reorganization;[54] however, both $\Delta S°$ and $\Delta H°$ decrease with pH, suggesting that these phenomena are correlated (Figures 5B and 6B).

It has been observed that backbone regions that are inadequately shielded to solvent interactions may be prone to water attack and may be involved in protein−protein interactions; these are usually called "dehydrons". We map these dehydrons into pFXN finding that they exist mainly in the "acid ridge" and the CTR. Notably, these dehydrons match the regions with the highest population of residues with a calculated shift in their pK_a making a link between this change in electrostatic surface potential and water interaction. Moreover, radial distribution analysis showed that in accordance with sorbitol results, the number of bound waters at high pHs is more than at lower pHs (Figure S14). Both results point to an important role of water molecules in this pH modulation of stability.

The activation parameters show that unfolding contributions are larger than the folding ones (Figure 5A). As shown in Figure 2A, unfolding rates increase with pH, indicating a decrease in the unfolding energy barrier height. This comes from the larger increase in $T\Delta S^{\ddagger}_u$ compared to $\Delta H^{\ddagger}_u$ that results in a lower activation energy. It is interesting to note that pK_a for the native state (Table 1) is ∼8.0, while the unfolding activation parameters have their strongest variation above pH 7. This suggests that the protonation above pH 7 and the

DOI: 10.1021/acs.jpcb.9b05960
J. Phys. Chem. B 2019, 123, 7676−7686

variation in the unfolding activation parameters are related. For the case of the folding reaction, the rate increases as pH decreases (Figure 2B), which is a consequence of the decrease in the folding activation energy coming, again, from the $T\Delta S_f^{\ddagger}$ and $\Delta H_f^{\ddagger}$ terms (Figure 5A). The strongest variation is ∼pH 6.0 which is close to the unfolded state pK_a (∼5.7). Interestingly, when the pH is approximately 6.0, the $\Delta H_f^{\ddagger}$ decrease and is ∼0. In this condition, both terms contribute positively to the barrier height. However, the almost absent enthalpic contribution makes the barrier mainly entropic. According to these observations, the variation of equilibrium thermodynamic parameters ($\Delta S°$ and $\Delta H°$) with pH is mostly contributed by the folding activation terms at low pH (∼pH 6.0−7.0), while variation comes from the unfolding activation terms at higher pH (∼pH 7.0−8.0).

pFXN folding rate constants (k_f) increase until a certain temperature depending on the pH reaches a maximum value and then decreases (Figure 4B). This behavior could be explained as a consequence of the change in the hydration shell surrounding the unfolded protein and transition states giving rise to an $\Delta C_{pf}^{\ddagger}$. Exposure of hydrophobic residues to the solvent when pFXN is unfolded influences the ordering of water molecules around the unfolded polypeptide chain.[55] As the temperature increases, these so-called "icebergs" are melted and after complete melting, the enthalpic dependency with temperature follows the $\Delta C_{pf}^{\ddagger}$. We observe that the temperature of maximum k_f decreases as pH increases from 6 to 8 (Figure 4B) as the polarity of the protein also increases. This might give rise to less stable water ordering as a consequence of the lower hydrophobic effect and in concordance with protein stability.

Dynamics of pFXN at the molecular level were analyzed using CpHMD,[56] showing that pK_a values of some residues in the native state are quite different from the reference values. Particularly, the "acid ridge" and flanking regions contain residues with marked pK_a shift, which among them are E18, E22, D27, E42, and E99 (Figure S15). It is noteworthy that the well-known relation of contact order and folding rate constants suggests that the high contact order interaction between D27 and E99, which brings together loop 1 with the first portion of the helix 2, could be implicated in folding rate dependence with pH. Moreover, the average RMSF, which is a measure of the global fluctuations of pFXN, points to a change in the nanosecond fluctuation dependence with pH (Figure 7A). Notably, the midpoint of this transition is nearby the pK_a values calculated for the native state. Thus, this opens up a question as to whether the effect on dynamics and stability is localized in a particular region or is distributed all over the structure.

Using structure-based models,[57] we observed that motions of C-terminus and loop 1 are correlated with their flanking loops.[58] Interestingly, these regions are rich in electrostatic interactions. Computationally calculated phi values, which are measures of nativeness of contacts in the transition state, of residues located in C-terminus and loop 1 are ∼0.3 (Figure S16). Thus, although contacts are mostly disrupted in the transition state, the fact that they are not zero and given the electrostatic nature of these interactions, suggest that pH could modulate their strength making possible that electrostatics affect the stability and folding dynamics of pFXN. The fact that FXN sequences from *E. coli* (eFXN) and pFXN are 55% identical provides evidence that subtle sequence differences may alter the folding mechanism because eFXN stability is not modulated by pH.[19,58] In this context, the important role of C-terminus and loop 1 in the stability of proteins from the FXN family is extensively discussed.[16,19,23,25] Then, it is not surprising that in the case of pFXN, the interactions concerning these regions were tunable by a charge shift, making stability modulated by pH.

In this work, we discussed the importance of electrostatics and their effects in thermodynamics and folding dynamics. We concluded that despite high sequence identity, FXN topology seems to be extremely malleable regarding the folding mechanisms. Thus, these differences may be reflected in the particular needs of the working conditions of these proteins. In the case of pFXN, the psychrophilic nature of the protein may have consequences in the mechanistic differences observed at different temperatures. While at 298 K it shows an important and singular pH effect for the kinetics and thermodynamics of this variant of FXN, the extrapolation to lower temperatures indicates that the effect of pH strongly diminishes, suggesting a correlation between physicochemical adaptation and evolution of the psychrophile organism. In this sense, we found no evident pattern that univocally correlates FXN sequences to temperature-adapted organisms such as psychrophilic or thermophilic organisms. In a previous publication from our laboratory, we compared *E. coli* FXN with the pFXN sequence, finding some differences in the amount of Gln and Asn residues and in the spatial distribution in the acidic residues.[22] Although we hypothesize that this may alter pH-dependent stability, we have no evidence of a relation of this with thermostability. As structurally most of solved variants are superimposable, we studied if there was structural evidence of temperature adaptation of pFXN to a cold environment. Then, we calculated local frustration using the Frustratometer Server[7,59] to analyze energetic conflicts in solved structures of psychrophile (*P. ingrahamii*, pFXN), mesophile (*E. coli*, eFXN), and thermophile (*Chaetomium thermophilum*, ctFXN) proteins from the FXN family. This calculation yielded that local frustration decreases as the optimal growth temperature increases; however, this is just one comparison making it just a coincidence (Figure S17). Most of these shifts in frustration occur among contacts located in the C-terminal of these proteins. In this sense, the field of quinary interactions of proteins has demonstrated that surface charged residues are important to modulate protein properties inside the cell.[60] Crowding effects and protein interactions need to be taken into account because diluted protein concentrations may give misleading information of what is going on in physiological environments. Future experiments pointing to the importance of charged residues in protein stability modulation and dynamics and in cell regulation are being performed.

■ ASSOCIATED CONTENT

Supporting Information

The Supporting Information is available free of charge on the ACS Publications website at DOI: 10.1021/acs.jpcb.9b05960.

Size-exclusion chromatography of purified pFXN; multiple sequence alignment of FXN variants; folding/unfolding denaturation, followed by both Trp fluorescence and far UV CD; representative time courses of folding and unfolding; pH dependencies of folding/unfolding denaturation at 298.15 K; REFER analysis; multiple perturbation: equilibrium experiments and kinetic experiments; cosolvent effects: protein hydration

DOI: 10.1021/acs.jpcb.9b05960
J. Phys. Chem. B 2019, 123, 7676−7686

changes during folding; constant pH and structure-based model simulations; water molecules bound to pFXN; X-ray structure of pFXN; calculation of phi values using structure-based model simulations free energy profile; and frustration profiles of *Psychromonas ingrahamii* (pFXN), Escherichia coli (eFXN), and Chaetomium thermophilum (ctFXN) (PDF)

AUTHOR INFORMATION

Corresponding Authors

*E-mail: lolo@qb.ffyb.uba.ar. Phone: +54 11 49648290 ext. 108. Fax: +54 11 49625457 (R.M.G.-L.).
*E-mail: ear@qb.fcen.uba.ar (E.A.R.).

ORCID

Rodolfo M. González-Lebrero: 0000-0002-3832-2270
Lucas Defelipe: 0000-0001-7859-7300
Carlos Modenutti: 0000-0001-5352-7234
Adrian E. Roitberg: 0000-0003-3963-8784
Nicolas A. Batastini: 0000-0002-0181-2954
Javier Santos: 0000-0002-1140-8234
Ernesto A. Roman: 0000-0001-9840-4115

Author Contributions

R.M.G.-L. and E.A.R. planned, performed, analyzed experiments, and wrote the manuscript. L.D. and A.E.R. designed and performed constant-pH molecular dynamics. C.M. performed constant-pH molecular dynamics. N.A.B. carried out the equilibrium experiments. M.E.N. performed and analyzed cosolvent experiments. R.M.G.-L., J.S., and E.A.R. designed and discussed the main ideas in this work.

Funding

This work was supported by the Agencia Nacional de Promoción Científica y Tecnológica (ANPCyT) (PICT 2013-0906 and PICT 2016-0014) and the Consejo Nacional de Investigaciones Científicas y Técnicas (CONICET) (PIP 2017-0732).

Notes

The authors declare no competing financial interest.

ACKNOWLEDGMENTS

We thank Dr. Ignacio E. Sánchez for insightful reading and suggestions.

REFERENCES

(1) Chung, H. S.; McHale, K.; Louis, J. M.; Eaton, W. A. Single-molecule Fluorescence Experiments Determine Protein Folding Transition Path Times. *Science* **2012**, *335*, 981−984.
(2) Dill, K. A.; MacCallum, J. L. The Protein-folding Problem, 50 years on. *Science* **2012**, *338*, 1042−1046.
(3) Chung, H. S.; Piana-Agostinetti, S.; Shaw, D. E.; Eaton, W. A. Structural Origin of Slow Diffusion in Protein Folding. *Science* **2015**, *349*, 1504−1510.
(4) Bryngelson, J. D.; Wolynes, P. G. Spin Glasses AND The Statistical Mechanics OF Protein Folding. *Proc. Natl. Acad. Sci. U.S.A.* **1987**, *84*, 7524−7528.
(5) Wolynes, P. G. Recent Successes of the Energy Landscape Theory of Protein Folding and Function. *Q. Rev. Biophys.* **2005**, *38*, 405−410.
(6) Oliveberg, M.; Wolynes, P. G. The Experimental Survey of Protein-Folding Energy Landscapes. *Q. Rev. Biophys.* **2005**, *38*, 245−288.
(7) Ferreiro, D. U.; Hegler, J. A.; Komives, E. A.; Wolynes, P. G. Localizing Frustration in Native Proteins and Protein Assemblies. *Proc. Natl. Acad. Sci. U.S.A.* **2007**, *104*, 19819−19824.
(8) Craig, P. O.; Lätzer, J.; Weinkam, P.; Hoffman, R. M. B.; Ferreiro, D. U.; Komives, E. A.; Wolynes, P. G. Prediction of Native-State Hydrogen Exchange from Perfectly Funneled Energy Landscapes. *J. Am. Chem. Soc.* **2011**, *133*, 17463−17472.
(9) Li, D. S.; Ohshima, K.; Jiralerspong, S.; Bojanowski, M. W.; Pandolfo, M. Knock-out of the cyaY Gene in Escherichia coli Does not Affect Cellular Iron Content and Sensitivity to Oxidants. *FEBS Lett.* **1999**, *456*, 13−16.
(10) Ahlgren, E.-C.; Fekry, M.; Wiemann, M.; Söderberg, C. A.; Bernfur, K.; Gakh, O.; Rasmussen, M.; Højrup, P.; Emanuelsson, C.; Isaya, G.; Al-Karadaghi, S. Iron-induced Oligomerization of Human FXN81-210 and Bacterial CyaY Frataxin and the Effect of Iron Chelators. *PLoS One* **2017**, *12*, No. e0188937.
(11) Prischi, F.; Pastore, C.; Carroni, M.; Iannuzzi, C.; Adinolfi, S.; Temussi, P.; Pastore, A. Of the Vulnerability of Orphan Complex Proteins: The Case Study of the E. coli IscU and IscS Proteins. *Protein Expr. Purif.* **2010**, *73*, 161−166.
(12) Shi, R.; Proteau, A.; Villarroya, M.; Moukadiri, I.; Zhang, L.; Trempe, J.-F.; Matte, A.; Armengod, M. E.; Cygler, M. Structural Basis for Fe-S Cluster Assembly and tRNA Thiolation Mediated by IscS Protein-Protein Interactions. *PLoS Biol.* **2010**, *8*, No. e1000354.
(13) Kim, J. H.; Bothe, J. R.; Frederick, R. O.; Holder, J. C.; Markley, J. L. Role of IscX in Iron-Sulfur Cluster Biogenesis in Escherichia coli. *J. Am. Chem. Soc.* **2014**, *136*, 7933−7942.
(14) Adinolfi, S.; Puglisi, R.; Crack, J. C.; Iannuzzi, C.; Dal Piaz, F.; Konarev, P. V.; Svergun, D. I.; Martin, S.; Le Brun, N. E.; Pastore, A. The Molecular Bases of the Dual Regulation of Bacterial Iron Sulfur Cluster Biogenesis by CyaY and IscX. *Front Mol. Biosci.* **2018**, *4*, 97.
(15) Faraj, S. E.; Venturutti, L.; Roman, E. A.; Marino-Buslje, C. B.; Mignone, A.; Tosatto, S. C. E.; Delfino, J. M.; Santos, J. The role of the N-terminal Tail for the Oligomerization, Folding and Stability of Human Frataxin. *FEBS Open Bio* **2013**, *3*, 310−320.
(16) Faraj, S. E.; González-Lebrero, R. M.; Roman, E. A.; Santos, J. Human Frataxin Folds Via an Intermediate State. Role of the C-Terminal Region. *Sci. Rep.* **2016**, *6*, 20782.
(17) Faraj, S. E.; Roman, E. A.; Aran, M.; Gallo, M.; Santos, J. The Alteration of the C-terminal Region of Human Frataxin Distorts its Structural Dynamics and Function. *FEBS J.* **2014**, *281*, 3397−3419.
(18) Roman, E. A.; Faraj, S. E.; Gallo, M.; Salvay, A. G.; Ferreiro, D. U.; Santos, J. Protein Stability and Dynamics Modulation: the CASE of human Frataxin. *PLoS One* **2012**, *7*, No. e45743.
(19) Adinolfi, S.; Nair, M.; Politou, A.; Bayer, E.; Martin, S.; Temussi, P.; Pastore, A. The Factors Governing the Thermal Stability of Frataxin Orthologues: How To Increase a Protein's Stability. *Biochemistry* **2004**, *43*, 6511−6518.
(20) Bonetti, D.; Toto, A.; Giri, R.; Morrone, A.; Sanfelice, D.; Pastore, A.; Temussi, P.; Gianni, S.; Brunori, M. The kinetics of Folding of Frataxin. *Phys. Chem. Chem. Phys.* **2014**, *16*, 6391−6397.
(21) Gianni, S.; Camilloni, C.; Giri, R.; Toto, A.; Bonetti, D.; Morrone, A.; Sormanni, P.; Brunori, M.; Vendruscolo, M. Understanding the Frustration Arising from the Competition Between Function, Misfolding, and Aggregation in a Globular Protein. *Proc. Natl. Acad. Sci. U.S.A.* **2014**, *111*, 14141−14146.
(22) Noguera, M. E.; Roman, E. A.; Rigal, J. B.; Cousido-Siah, A.; Mitschler, A.; Podjarny, A.; Santos, J. Structural Characterization of Metal Binding to a Cold-adapted Frataxin. *J. Biol. Inorg Chem.* **2015**, *20*, 653−664.
(23) Noguera, M. E.; Aran, M.; Smal, C.; Vazquez, D. S.; Herrera, M. G.; Roman, E. A.; Alaimo, N.; Gallo, M.; Santos, J. Insights on the Conformational Dynamics of Human Frataxin through Modifications of loop-1. *Arch. Biochem. Biophys.* **2017**, *636*, 123−137.
(24) Correia, A. R.; Wang, T.; Craig, E. A.; Gomes, C. M. Iron-binding activity in yeast frataxin entails a trade off with stability in the $\alpha 1/\beta 1$ acidic ridge region. *Biochem. J.* **2010**, *426*, 197−203.
(25) Roman, E. A.; Faraj, S. E.; Cousido-Siah, A.; Mitschler, A.; Podjarny, A.; Santos, J. Frataxin from Psychromonas Ingrahamii as a Model to Study Stability Modulation within the CyaY Protein Family. *Biochim. Biophys. Acta* **2013**, *1834*, 1168−1180.

DOI: 10.1021/acs.jpcb.9b05960
J. Phys. Chem. B 2019, 123, 7676−7686

(26) Yamaoka, K.; Nakagawa, T.; Uno, T. Application of Akaike's information criterion (AIC) in the evaluation of linear pharmacokinetic equations. *J. Pharmacokinet. Biopharm.* **1978**, *6*, 165−175.
(27) Salomon-Ferrer, R.; Götz, A. W.; Poole, D.; Le Grand, S.; Walker, R. C. Routine Microsecond Molecular Dynamics Simulations with AMBER on GPUs. 2. Explicit Solvent Particle Mesh Ewald. *J. Chem. Theory Comput.* **2013**, *9*, 3878−3888.
(28) Hornak, V.; Abel, R.; Okur, A.; Strockbine, B.; Roitberg, A.; Simmerling, C. Comparison of Multiple Amber Force Fields and Development of Improved Protein Backbone Parameters. *Proteins: Struct. Funct. Bioinf.* **2006**, *65*, 712−725.
(29) Meng, Y.; Roitberg, A. E. Constant pH Replica Exchange Molecular Dynamics in Biomolecules Using a Discrete Protonation Model. *J. Chem. Theory Comput.* **2010**, *6*, 1401−1412.
(30) Noel, J. K.; Whitford, P. C.; Sanbonmatsu, K. Y.; Onuchic, J. N. SMOG@ctbp: Simplified Deployment of Structure-Based Models in GROMACS. *Nucleic Acids Res.* **2010**, *38*, W657−W661.
(31) Clementi, C.; Nymeyer, H.; Onuchic, J. N. Topological and energetic factors: what determines the structural details of the transition state ensemble and "en-route" intermediates for protein folding? an investigation for small globular proteins. *J. Mol. Biol.* **2000**, *298*, 937−953.
(32) Kumar, S.; Rosenberg, J. M.; Bouzida, D.; Swendsen, R. H.; Kollman, P. A. The Weighted Histogram Analysis Method for Free-Energy Calculations on Biomolecules. I. The Method. *J. Comput. Chem.* **1992**, *13*, 1011−1021.
(33) Cho, S. S.; Levy, Y.; Wolynes, P. G. P versus Q: Structural Reaction Coordinates Capture Protein Folding on Smooth Landscapes. *Proc. Natl. Acad. Sci. U.S.A.* **2006**, *103*, 586−591.
(34) Kiefhaber, T.; Sánchez, I. E.; Bachmann, A. Characterization of Protein Folding Barriers with Rate Equilibrium Free Energy Relationships. In *Protein Folding Handbook*; Buchner, J., Kiefhaber, T., Eds.; Weinheim, Germany: Wiley-VCH Verlag GmbH, 2005; pp 411−444.
(35) Myers, J. K.; Nick Pace, C.; Martin Scholtz, J. Denaturantmvalues and heat capacity changes: Relation to changes in accessible surface areas of protein unfolding. *Protein Sci.* **1995**, *4*, 2138−2148.
(36) Tanford, C. Protein Denaturation. *Adv. Protein Chem.* **1968**, *23*, 121−282.
(37) Tanford, C. Protein Denaturation. *Adv. Protein Chem.* **1970**, *24*, 1−95.
(38) Hagen, S. J. Solvent viscosity and friction in protein folding dynamics. *Curr. Protein Pept. Sci.* **2010**, *11*, 385−95.
(39) Hänggi, P.; Talkner, P.; Borkovec, M. Reaction-rate Theory: Fifty Years after Kramers. *Rev. Mod. Phys.* **1990**, *62*, 251−341.
(40) Kramers, H. A. Brownian Motion in a Field of Force and the Diffusion Model of Chemical Reactions. *Physica* **1940**, *7*, 284−304.
(41) Ansari, A.; Jones, C.; Henry, E.; Hofrichter, J.; Eaton, W. The Role of Solvent Viscosity in the Dynamics Of Protein Conformational Changes. *Science* **1992**, *256*, 1796−1798.
(42) Placenti, M. A.; Kaufman, S. B.; González Flecha, F. L.; González Lebrero, R. M. Unexpected Effects of K+ and Adenosine Triphosphate on the Thermal Stability of Na+,K+-ATPase. *J. Phys. Chem. B* **2017**, *121*, 4949−4957.
(43) Perl, D.; Jacob, M.; Bánó, M.; Stupák, M.; Antalík, M.; Schmid, F. X. Thermodynamics of a Diffusional Protein Folding Reaction. *Biophys. Chem.* **2002**, *96*, 173−190.
(44) Makhatadze, G. I.; Privalov, P. L. Energetics of Protein Structure. *Adv. Protein Chem.* **1995**, *47*, 307−425.
(45) Miyawaki, O. Hydration State Change of Proteins Upon Unfolding in Sugar Solutions. *Biochim. Biophys. Acta* **2007**, *1774*, 928−935.
(46) Xie, G.; Timasheff, S. N. Mechanism of the stabilization of ribonuclease A by sorbitol: preferential hydration is greater for the denatured then for the native protein. *Protein Sci.* **2008**, *6*, 211−221.
(47) Plaza del Pino, I. M.; Sanchez-Ruiz, J. M. An Osmolyte Effect on the Heat Capacity Change for Protein Folding. *Biochemistry* **1995**, *34*, 8621−8630.
(48) de Oliveira, G. A. P.; Silva, J. L. A hypothesis to Reconcile the Physical and Chemical Unfolding of Proteins. *Proc. Natl. Acad. Sci. U.S.A.* **2015**, *112*, E2775−E2784.
(49) Lange, O. F.; Grubmüller, H. Generalized correlation for biomolecular dynamics. *Proteins: Struct., Funct., Bioinf.* **2005**, *62*, 1053−1061.
(50) Hünenberger, P. H.; Mark, A. E.; Van Gunsteren, W. F. Fluctuation and Cross-Correlation Analysis of Protein Motions Observed in Nanosecond Molecular Dynamics Simulations. *J. Mol. Biol.* **1995**, *252*, 492−503.
(51) Parker, M. J.; Spencer, J.; Clarke, A. R. An Integrated Kinetic Analysis of Intermediates and Transition States in Protein Folding Reactions. *J. Mol. Biol.* **1995**, *253*, 771−786.
(52) Sánchez, I. E.; Kiefhaber, T. Non-linear Rate-Equilibrium Free Energy Relationships and Hammond Behavior in Protein Folding. *Biophys. Chem.* **2003**, *100*, 397−407.
(53) Bodenreider, C.; Kiefhaber, T. Interpretation of Protein Folding ψ Values. *J. Mol. Biol.* **2005**, *351*, 393−401.
(54) Liu, L.; Yang, C.; Guo, Q.-X. A study on the enthalpy-entropy compensation in protein unfolding. *Biophys. Chem.* **2000**, *84*, 239−251.
(55) Oliveberg, M.; Tan, Y. J.; Fersht, A. R. Negative Activation Enthalpies in the Kinetics of Protein Folding. *Proc. Natl. Acad. Sci. U.S.A.* **1995**, *92*, 8926−8929.
(56) Swails, J. M.; York, D. M.; Roitberg, A. E. Constant pH Replica Exchange Molecular Dynamics in Explicit Solvent Using Discrete Protonation States: Implementation, Testing, and Validation. *J. Chem. Theory Comput.* **2014**, *10*, 1341−1352.
(57) Whitford, P. C.; Noel, J. K.; Gosavi, S.; Schug, A.; Sanbonmatsu, K. Y.; Onuchic, J. N. An all-atom structure-based potential for proteins: Bridging minimal models with all-atom empirical forcefields. *Proteins: Struct., Funct., Bioinf.* **2009**, *75*, 430−441.
(58) Brown, D. K.; Penkler, D. L.; Sheik Amamuddy, O.; Ross, C.; Atilgan, A. R.; Atilgan, C.; Tastan Bishop, Ö. MD-TASK: a software suite for analyzing molecular dynamics trajectories. *Bioinformatics* **2017**, *33*, 2768−2771.
(59) Parra, R. G.; Schafer, N. P.; Radusky, L. G.; Tsai, M.-Y.; Guzovsky, A. B.; Wolynes, P. G.; Ferreiro, D. U. Protein Frustratometer 2: a Tool to Localize Energetic Frustration in Protein Molecules, now with Electrostatics. *Nucleic Acids Res.* **2016**, *44*, W356−W360.
(60) Cohen, R. D.; Pielak, G. J. Electrostatic Contributions to Protein Quinary Structure. *J. Am. Chem. Soc.* **2016**, *138*, 13139−13142.

DOI: 10.1021/acs.jpcb.9b05960
J. Phys. Chem. B 2019, 123, 7676−7686